International Journal of Pharmacology

ISSN 1811-7775

science alert

ansinet
Asian Network for Scientific Information

OPEN ACCESS International Journal of Pharmacology

ISSN 1811-7775
DOI: 10.3923/ijp.2023.810.824

Research Article
Synthesis of New 1,4-Dihydropyridine Scaffold Thiadiazole and Triazole Moiety and *in silico* Molecular Interaction Study of SARS-CoV-2 M^{pro} and ACE2 Protease

[1]Radhakrishnan Surendrakumar, [2]Pitchai Sangan, [1]Akbar Idhayadhulla, [3]Anis Ahamed and [3]Reham M. Alahmadi

[1]Department of Chemistry, Nehru Memorial College, Affiliated to Bharathidasan University, Puthanampatti, Tamil Nadu 321007, South India
[2]Hyprocell Biotech Company, Branford, Connecticut 06405, United States of America
[3]Department of Botany and Microbiology, College of Sciences, King Saud University, P.O. Box 2455, Riyadh 11451, Saudi Arabia

Abstract

Background and Objective: In this work, the synthesis of 1,4-dihydropyridine based bioactive compounds for computational study with SARS-CoV-2 M^{pro} (PDB ID: 6y2f) and ACE2 (6M0J). **Materials and Methods:** A series of novel 1,4-dihydropyridine appended compounds (3a-3g and 4a-4g) were prepared through Hantzsch reaction and followed by amination method. The newly prepared compounds were satisfactorily analysed by CHN analysis and various spectroscopic (IR, ^{1}H NMR, ^{13}C NMR and mass) tools. The compounds of remdesivir, hydroxychloroquine and CQ were optimized by Dmol^{3} Materials Studio software 2017. *In silico* study was executed to forecast binding efficiency of 3a-3g and 4a-4g with targeted receptor spike protein (host angiotensin-converting enzyme 2; ACE2; 6M0J) and SARS-CoV-2 main protease (6y2f). **Results:** The binding energy of the docked compounds (3a-3g), remdesivir, hydroxychloroquine and chloroquine was observed at -5.89, -6.74, -6.58, -6.38, -6.76, -5.83, -5.54, -4.40, -5.22 and -5.41 Kcal mol^{-1}, respectively. The binding energies of the docked compounds (4a-4g), RDV, HQ and CQ were observed at -7.14, -6.62, -6.89, -6.60, -7.71, -6.55 and -6.52 Kcal mol^{-1}, respectively. The results confirmed that the presence electron withdrawing groups on benzene such as nitro and chloro- substitutions or free benzene enhancement of the inhibitory behavior on SARS-CoV-2 M^{pro}. **Conclusion:** The present data of synthesized compounds 3a-3g and 4a-4g showed significant binding ability with this protease receptor and better than remdesivir (RDV), chloroquine (CQ) and hydroxychloroquine (HQ). Chloroquine (CQ) and compounds (3c), (4a), (4b), (4e) and (4f) exhibited good interaction with ACE2 receptor.

Key words: 1,4-Dihydropyridine, thiadiazole, oxadiazole, triazole, molecular docking, SARS-CoV-2 M^{pro} and ACE2, structure activity relationship

Citation: Surendrakumar, R., P. Sangan A. Idhayadhulla, A. Ahamed and R.M. Alahmadi, 2023. Synthesis of new 1,4-dihydropyridine scaffold thiadiazole and triazole moiety and *in silico* molecular interaction study of SARS-CoV-2 M^{pro} and ACE2 protease. Int. J. Pharmacol., 19: 810-824.

Corresp onding Author: Radhakrishnan Surendrakumar, Department of Chemistry, Nehru Memorial College, Affiliated to Bharathidasan University, Puthanampatti, Tamil Nadu 321007, South India

Competing Interest: The authors have declared that no competing interest exists.

Data Availability: All relevant data are within the paper and its supporting information files.

INTRODUCTION

In present year, the development of novel antiviral drug is one of the most well-known research areas in medicinal chemistry. Diseases caused by viral infection are main civic health issue[1]. A positive strand RNA infection caused the virus disease which began in China and has become a global epidemic[2-5]. The coronavirus COVID-19 is affecting almost all countries (above 200) and territories around the world. It is urgent to begin successful antivirals and curative medicine. A vaccine for SARS-CoV-2 (Sputnik V) was approved by Russia on August 11, 2020. An extensive research effort is being undertaken to develop and repurpose new drugs that target different components of the virus[6]. Russian scientists developed an adenovirus vaccine based on two adenovirus vectors[7]. Some viral proteins are over 90% homologous to those found in the earlier SARS Corona Virus (SARS-CoV) and the viral genome is 82% identical[8]. Producing nonstructural proteins for viral replication using SARS-CoV-2[9-11]. A specific protease inhibitor can be designed in the absence of a homologous human protease[12]. Pyridine skeleton attracts more important among chemists and biologists because of its abundance in nature. Some of the pyridines exhibited good antitumor, antiviral activities, antifungal[13,14]. In the area of drugs and pharmaceuticals, (DHPs) are among the most important compounds[15,16]. They reduce laboratory operations and solvent quantities, as well as their cost, in synthetic organic chemistry[17,18]. Variations in the structural model increased behavior of pyridine derivatives[19-21]. For example, they are analogues of hydrogenised coenzymes[22] calcium channel blockers, anticoagulant[23] and act as multidrug resistance[24], multi compound synthesis[25,26]. The SARS-CoV-2 ribbon structure and three-dimensional catalytic activity center are reported by Bosica and Abdilla[27].

Recent reports suggest that pyridine analogues useful pharmacologically effective[27,28]. The DHP molecule exhibited antimicrobial, anticancer[29-31] and antiviral activities are reported. Significant biological actions of thiosemicarbazide include antineoplastic activity[32]. There are numerous ways to study the interactions among hydrazines, esters and thiosemicarbazide[33]. In scrutiny of these comments, we plan to match up the new pyridine analogues and different substitutions of five membered heterocyclic compounds in activity level. The substituted compound of thiosemicarbazide and semicarbazide reacted with both H_2SO_4 and NaOH[34]. In this research, synthesis a new series of 1,4-dihydropyridine derivatives, screened for computational study analysis against SARS-CoV-2 M^{pro} (PDB ID: 6y2f) and ACE2 (6M0J) receptors for designing new anti-corona agents.

MATERIALS AND METHODS

Study area: The study was taken place in Research Department of Chemistry, Nehru Memorial College (Affiliated to Bharathidasan University), Puthanampatti, Trichy, India. From April, 2022 to October, 2023.

Material and reagents: Melting points were noted. The IR spectra were captured using a Shimadzu 8201pc (4000-400 cm^{-1}) and recorded in kBr. The Bruker DRX-300 MHz was used to record the 1H and 13C NMR spectra. The Clarus SQ8 (EI) GCMS from PerkinElmer captured mass spectra. An Elementary analyzer model (Varian EL III) was used to record the elemental analyses (CHN).

Synthesis of compounds (3a-3g): A general method for synthesis of 3a-3g, compound 2 (0.01 mol, 3.7g) and 4 mL of Concentration. The H_2SO_4 stirred well for 20-30 min and added few drops of ammonia solution, the obtained solid was purified using ethanol. The reaction was monitored by TLC, yield: 75-85%. Hexane was used as solvents in TLC. Thin-layer chromatography (TLC) was done by CCM Gel de silica gel 60 F254 sheet (0.1 mm) with hexane as emerging eluent. The compounds were detected passing an E-Series UV hand lamp (254/365 nm wavelength). The compounds are purified by column chromatography (gel filtration method, wet condition) and silica gel (60-120 mesh) was used as a sorbent. Same synthetic procedure was used for synthesis of the 3b-3g.

Compound (3a): The IR (kBr, cm^{-1}): 3415 (N-Hstr), 2929 (CH-str furyl ring), 2972 (NH_2), 1646 (C=N), 653 (C-O-C). The ^{1}H NMR (300MHz, DMSO-d_6): δppm: 10.13 (s, 1H, C =N-NH), 7.29 (s, 4H, oxadiazol-NH_2), 6.25 (dd, 3H, J= 3.2, one more J value, Furyl), 5.02 (s, 1H, CH, Py), 2.27 (s, 6H, 2-CH_3, Py). The ^{13}CNMR (75 MHz, DMSO-d_6): δ, ppm 169.7 (2C, C-NH_2), 164.0 (2C, oxadiazol),152.8, 142.8, 110.7, 106.7 (4C, furyl), 130.6, 107.3, 44.7 (5C, pyridine), 15.0 (2C-CH_3,Py). The EI-MS (Relative intensity (%)): m/z 342.34 (M^+, 20). Anal. Calc. for $C_{15}H_{15}N_7O_3$: C, 52.78; H, 4.43; N, 28.73; Found: C, 52.76; H, 4.45; N, 28.75. M. pt.: 257-260°C. Brown color solid and Yield: 62%.

Compound (3b): The IR (kBr, cm^{-1}): 3420(N-Hstr), 2956(NH_2), 1741 (C=N), 802(Ar-H), 660(C-O-C). The ^{1}HNMR(300 MHz, DMSO-d_6): δ(ppm): 10.16(s, 1H, C=N-NH), 6.99(s, 4H, oxadiazol-NH_2), 7.33-7.28(m, 5H, Ph-ring), 4.43(s, 1H, CH-Py), 2.30(s, 6H, 2-CH_3, Py). The ^{13}CNMR(75 MHz, DMSO-d_6): 169.8(2C, C-NH_2), 164.1(2C, oxadiazol), 144.8-127.1(6C, phenyl ring), 131.6, 108.3, 43.1(5C, in pyridine ring), 16.0(2C, C-CH_3, Py). The EI-MS (Relative intensity (%)): m/z 351.36(M^+, 23%). Anal. Cal. for $C_{17}H_{17}N_7O_2$: C, 58.11; H, 4.88; N, 27.90; Found: C, 58.13; H, 4.90; N, 27.92. White powder, Mp:150°C and Yield: 65%.

Compound (3c): The IR (kBr, cm^{-1}): 3428(N-H), 2982(NH_2), 1656(C=N), 840(C-Cl), 805(Ar-H), 645(C-O-C). The ^{1}HNMR(DMSO-d_6), δ(ppm): 10.15(s, 1H, C=N-NH), 6.98(s, 4H, oxadiazol-NH_2), 7.36-7.19(m, 4H, Ph-ring) 5.02(s, 1H, CH-Py), 2.24(s, 6H, 2-CH_3, Py). The ^{13}CNMR(75MHz, DMSO-d_6): 169.7(2C, C-NH_2), 164.0(2C, oxadiazol), 142.5, 131.4, 130.8, 128.1(6C, Ph-Cl), 130.7, 107.4, 43.7(5C, in pyridine ring), 15.1(2C, C-CH_3, Py). The EI-MS (Relative intensity (%)): m/z 385.80(M^+, 17). Anal. Cal. for $C_{17}H_{16}ClN_7O_2$: C, 52.92; H, 4.17; N, 25.41; Found: C, 52.94; H, 4.20; N, 25.43. White powder, Mp: 142°C and Yield: 62%.

Compound(3d): The IR(kBr, cm^{-1}): 3420(N-H), 2980(NH_2), 1645(C=N), 1448(C-O-H), 815(Ar-H), 662(C-O-C). The ^{1}HNMR(DMSO-d_6), δ(ppm): 10.20(s, 1H, C=N-NH), 9.47(s, 1H, C-OH), 7.45(s, 4H, oxadiazol, NH_2), 6.34-7.07(m, 4H, Ph-ring), 5.06(s, 1H, CH-Py), 2.26(s, 6H, 2-CH_3, Py). The ^{13}C NMR(75MHz, DMSO-d_6): 168.7(2C, C-NH_2), 163.0(2C, oxadiazol), 156.6, 138.2, 131.2, 130.2(5C, Ph-ring), 116.2(1C, Ph-OH), 130.7, 106.3, 43.7(5C, in pyridine ring), 15.3(2C-CH_3, Py). The EI-MS(Relative intensity (%)): m/z 367.36(M^+, 20). Anal.Cal. for $C_{17}H_{17}N_7O_3$: C, 55.58; H, 4.66; N, 26.69; Found: C, 55.60; H, 4.68; N, 26.70. White powder, Mp: 126°C and Yield: 46%.

Compound (3e): The IR (kBr, cm^{-1}): 3419(N-H), 2982(NH_2), 1651(C=N), 1540(C-NO_2), 812 (Ar-H), 641(C-O-C). ^{1}HNMR(DMSO-d_6), δ(ppm): 10.12(s, 1H, C=N-NH), 8.13-7.47(m, 4H, Ph-ring), 7.36(s, 4H, oxadiazol, NH_2), 5.03(s, 1H, CH-Py), 2.28(s, 6H, 2-CH_3, Py). The ^{13}CNMR(75MHz, DMSO-d_6):168.7(2C, C-NH_2), 165.0(2C, oxadiazol), 151.4, 144.8, 126.9, 123.6(6C, Ph-NO_2), 130.5, 107.5, 44.7(5C, in pyridine ring), 15.1(2C-CH_3, Py). The EI-MS (Relative intensity (%)): m/z 396.36(M^+, 21). Anal.Cal. for $C_{17}H_{16}N_8O_4$: C, 51.52; H, 4.07; N, 28.27; Found: C, 51.53; H, 4.09; N, 28.55. Pale yellow, Mp: 141°C and Yield: 52%.

Compound (3f): The IR (kBr, cm^{-1}): 3422(N-H), 3020(Ar-H), 2970(NH_2), 2961(C-Hstr of CH_3), 1641(C=N), 652 (C-O-C). The ^{1}HNMR(DMSO-d_6), δ(ppm): 10.16(s, 1H, C=N-NH), 7.38(s, 4H, oxadiazol, NH_2), 6.86-7.18(m, 4H, Ph-ring), 5.06(s, 1H, CH-Py), 3.86(s, 3H, -OCH_3), 2.25(s, 6H, 2-CH_3). The ^{13}CNMR(75MHz, DMSO-d_6): 165.73(2C, C-NH_2), 164.01(2C, oxadiazol), 157.2, 135.9, 114.6, 129.3(6C, Ph-ring), 130.6, 107.4, 46.4(5C, in pyridine ring), 55.7(1C, Ph-OCH_3), 44.6(1C, in pyridine -ring), 16.0(2C-CH_3, Py). The EI-MS (Relative intensity (%)): m/z 381.38 (M^+, 19). Anal.Cal. for $C_{18}H_{19}N_7O_3$: C, 56.69; H, 5.02; N, 25.71; Found: C, 56.70; H, 5.04; N, 25.72. White powder, Mp: 125°C and Yield: 60%.

Compound (3g): The IR (kBr, cm^{-1}): 3426(N-H), 2973(NH_2), 2956(C-Hstr of CH_3), 1656(C=N), 810(Ar-H), 656(C-O-C). The ^{1}HNMR(DMSO-d_6), δ(ppm): 10.18(s, 1H, C=N-NH), 7.29(s, 4H, oxadiazol, NH_2), 7.28-7.23(m, 4H, Ph-ring) 5.08(s, 1H, CH-Py), 3.12 (s, 6H, -$N(CH_3)_2$), 2.41 (s, 6H, 2-CH_3). The ^{13}C NMR(75MHz, DMSO-d_6): 168.7(2C, C-NH_2), 164.1(2C-oxadiazol), 134.8, 132.9, 126.9, 126.6(6C, Ph), 135.5, 107.5, 44.6(5C, in pyridine-ring), 40.8(2C, $N(CH_3)_2$), 16.0 (2C-CH_3, Py). The EI-MS (Relative intensity (%)): m/z 350.35(M^+, 16). Anal. Cal for $C_{19}H_{22}N_7O_2$: C, 58.28; H-4.60; N-27.99; Found: C, 58.30; H, 4.62; N, 27.10. White powder, Mp: 110°C and Yield: 46%.

General procedure for synthesis of (4a-4g)

A detailed procedure was given in supplementary file: The compound 2 (0.01 mol, 3.7 g) and 2N NaOH in ethanol (15 mL) was refluxed for 5 hrs then acidified with dil. The HCl (10 mL) and purified using ethanol.

Compound (4a): The IR (kBr, cm^{-1}): 3342(N-H-pyridine ring), 3240(N-H-triazole ring) 3098(OH), 2930(CH-str furyl ring), 658(C-O-C). The ^{1}HNMR(DMSO-d_6), δ(ppm): 10.83(s, 2H, OH), 8.98(s, 1H, C=N-NH), 7.39, 6.30(d, 3H, J=6.4Hz, Furyl), 5.82(s, 1H, CH, Py), 4.43(s, 2H, NH-in triazole), 2.50(s, 6H, 2CH_3). The ^{13}CNMR(75 MHz, DMSOd_6): 161.3(2C, COH), 151.1, 145.8, 110.3, 106.7(4C, Furyl-ring), 146.4(2C, triazol), 137.3, 110.3, 44.6(5C, in pyridine-ring), 16.9(2C-CH_3, Py). The EI-MS (Relative intensity (%)): m/z 341.71(M^+, 13). Anal. Cal. for $C_{15}H_{15}N_7O_3$: C, 52.78; H, 4.43; N, 28.73; Found: C, 52.70; H, 4.41; N, 28.71. Light brown colour, Mp: 126°C and Yield: 52%.

Compound (4b): The IR (kBr, cm^{-1}); 3355(N-H-pyridine ring), 3256(N-H-triazole ring), 3092(OH in triazole ring), 3034(Ar-H), 921(aromatic CH str). The ^{1}HNMR(DMSO-d_6), δ(ppm): 10.81(s, 2H, OH), 8.96 (s, 1H, C=N-NH), 7.40-7.26 (m, 5H, Ph-ring), 5.85(s, 1H, 4CH, Py), 4.46(s, 2H, NH-triazole), 2.57(s, 6H, 2 CH_3). The ^{13}CNMR(75MHz, DMSO-d_6):161.3(2C-OH), 149.7, 125.5, 123.5(6H, Phenyl ring), 146.6(2C, triazole), 135.3, 102.3, 43.6(5C, in pyridine ring), 15.9(2C-CH_3, Py). The EI-MS (Relative intensity (%)): m/z 351.36 (M^+, 17). Anal.Cal. for $C_{17}H_{17}N_7O_2$: C, 58.11; H, 4.88; N, 27.90; Found: C, 58.13; H, 4.90; N, 27.92. White powder, Mp: 187°C and Yield: 53%.

Compound (4c): The IR (kBr, cm^{-1}): 3349(N-H-pyridine ring), 3250(N-H-triazole ring), 3091(OH in triazole ring), 923(aromatic CH str), 839(C-Cl). The ^{1}HNMR(DMSO-d_6), δ(ppm): 10.88(s, 2H, OH), 8.88(s, 1H, C=N-NH), 7.38-7.26(m, 4H, Ph-ring), 5.83(s, 1H, CH, Py), 4.46(s, 2H, NH-in triazole) 2.53(s, 6H, 2-CH_3). The ^{13}CNMR(75MHz, DMSO-d_6):162.35(2C-OH), 146.4(2C, triazole), 142.8(1C, Ph-Cl), 140.3, 136.0-124.5(5C, Ph-ring), 135.36, 106.35, 47.63(5C, in pyridine ring), 15.88(2C-CH_3, Py). The EI-MS (Relative intensity (%)): m/z 385.80(M^+, 13). Anal.Cal. for $C_{17}H_{16}ClN_7O_2$: C, 52.92; H, 4.18; N, 25.41; Found: C, 52.95; H, 4.20; N, 25.42. White powder, Mp: 156°C and Yield: 43%.

Compound (4d): The IR (kBr, cm^{-1}); 3344(N-H-pyridine ring), 3249(N-H-triazole ring), 3086(OH in triazole ring), 1449(C-OH in phenyl ring), 926(aromatic CH str). The ^{1}HNMR(DMSO-d_6), δ(ppm): 10.68(s, 3H, C-OH), 8.99(s, 1H, C=N-NH), 7.20-6.39(m, 4H, Ph-ring), 5.86(s, 1H, CH, Py), 4.47(s, 2H, NH-in triazole), 2.53(s, 6H, 2-CH_3). The ^{13}CNMR(75MHz, DMSO-d_6): 163.3(2C-OH), 152.7(1C, Ph-OH) 146.3(2C, triazole)142.4, 134.2, 117.5(5C, Ph-OH), 135.3, 103.3, 47.6(5C, in pyridine ring), 16.9(2C-CH_3, Py). The EI-MS (Relative intensity (%): m/z 367.36(M^+, 13). Anal.Cal. for $C_{17}H_{17}N_7O_3$: C, 55.58; H, 4.66; N, 26.69; Found: C, 55.60; H, 4.68; N, 26.71.Pale yellow, Mp:141°C and Yield: 52%.

Compound (4e): The IR (kBr, cm^{-1}) 3340(N-H-pyridine ring), 3249(N-H-triazole ring), 3086(OH), 1540(C-NO_2), 932(aromatic CH str). The ^{1}HNMR(DMSO-d_6), δ(ppm): 10.86(s, 2H, OH), 8.92(s, 1H, C=N-NH), 8.19-7.50(m, 4H, Ph-ring), 5.80(s, 1H, 4CH, Py), 4.40(s, 2H, NH-in triazole) 2.59(s, 6H, 2CH_3). The ^{13}CNMR (75MHz, DMSO-d_6): 166.3(2C-OH), 155.8, 145.3, 128.3, 120.5, (6C, Ph-NO_2), 146.7(2C, triazole), 130.3, 107.3, 44.6(4C, in pyridine ring), 16.9(2C, CH_3, Py). The EI-MS (Relative intensity (%)): m/z 396.36(M^+, 24); Anal.Cal. for $C_{17}H_{16}N_8O_4$: C, 51.51; H, 4.07; N, 28.27; Found: C, 51.52; H, 4.09; N, 28.29. Pale yellow, Yield: 51% and Mp: 140°C.

Compound (4f): The IR (kBr, cm^{-1}); 3355(N-H-pyridine ring), 3252(N-H-triazole ring), 3079 (OH), 2966(C-H str of CH_3), 932(aromatic CH str), 658(C-O-C). The ^{1}HNMR(DMSO-d_6), δ(ppm): 10.79(s, 2H, OH) , 8.95(s, 1H, C=N-NH), 6.80-7.30(m, 4H, Ph-ring), 5.87(s, 1H, CH, Py), 4.46(s, 2H, NH-in triazole) 3.83(s, 3H, -OCH_3), 2.55(s, 6H, 2-CH_3). The ^{13}CNMR(75MHz, DMSOd_6):163.4(2C-OH), 157.8-130.5(6C, Ph ring), 146.2(2C, triazole), 135.3, 102.3(4C, in pyridine ring), 55.9(1C, Ph-OCH_3), 44.6(1C, in pyridine ring), 16.9(2C-CH_3, Py). The EI-MS (Relative intensity (%)): m/z 381.38(M^+, 16); Anal.Cal. for $C_{18}H_{19}N_7O_3$: C, 56.69; H, 5.02; N, 25.71; Found: C, 56.70%; H, 5.05; N, 25.73. White powder, Mp: 128°C and Yield: 56%.

Compound (4g): The IR (kBr, cm^{-1}); 3343(N-H-pyridine ring), 3246(N-H-triazole ring), 3082(OH), 2953(C-H str of CH_3), 932(aromatic CH str), 659(C-O-C). The ^{1}HNMR(DMSO-d_6), δ(ppm): 10.86(s, 2H, OH), 8.86(s, 1H, C =N-NH), 7.40-7.15(m, 4H, Ph-ring), 5.77(s, 1H, CH, Py), 4.46(s, 2H, NH-in triazole), 3.18(s, 6H, -N(CH_3), 2.52(s, 6H, 2-CH_3, Py). The ^{13}CNMR(75MHz, DMSO-d_6):166.3(2C-OH), 146.9, 136.6, 130.6, 113.5(6C, Ph), 146.5(2C, triazole), 133.3, 109.4, 44.6 (5C, in pyridine ring), 40.5(2C, N(CH_3)$_2$), 16.9(2C-CH_3, Py). The EI-MS (Relative intensity (%)): m/z 350.35 (M^+, 19). Anal.Cal. for $C_{19}H_{22}N_8O_2$: C, 58.28; H, 4.60; N, 27.95; Found: C, 58.29; H, 4.62; N, 27.97. White powder, Mp: 182°C and Yield: 60%.

Molecular docking analysis

Computational study of compounds with SARS-CoV-2 M^{pro} (PDB ID: 6y2f) and ACE2 (PDB ID: 6M0J): To optimize compound structures, we used Material Studio software 2017 via DMol^3 module and structures were calculated by task; geometry optimization, electronic; DND (double numerical plus d-function), Basis set; 3.5 and max SCF (shell self-consistent field) cycles; 999. In next stage, structures were saved mol2 after optimization. The 3D view of coronavirus (SARS-CoV-2) proteins with PDB ID: 6y2f, ACE2 PDB ID: 6M0J were acquired from RCSB Protein Data Bank (PDB). The FDA approved anti-corona drugs including chloroquine, HQ and RDV were retrieved from PubChem. AutoDock version 1.5.6. Program was used to interact between compounds and receptors. For visualization and interactions, the Discovery Studio 2016 was used. All docking simulations were performed using a grid box (x, y and z directions) with 126×126×126 Å points with a grid-point spacing of 0.5138 Å for 6y2f and a grid box (x, y and z directions) with 126×126×126 Å points with a grid-point spacing of 0.5138 Å for 6M0J. Lamarckian genetic algorithm (LGA) method with the 100 runs was applied in AutoDock 4.2 calculations.

RESULTS AND DISCUSSION

Synthesis and characterization of compounds: The compounds 1 and 2 were synthesized according to the literature method[38]. Compounds (3a-3g) and (4a-4g) were prepared by reacting compound 2 with H_2SO_4/NH_3 (for 3a-3g) and NaOH/dil.HCl (for 4a-4g) by cyclization method. The sequential syntheses of compounds 3a-3g and 4a-4g were given in Scheme 1.

The compounds (3a-3g)'s IR spectra revealed an absorption band at 3426-3349 cm^{-1} due to N-H str and NH_2 band at 2980 to 290 cm^{-1}. The band at 1646-1656 cm^{-1} due to C=N str and 656-653 cm^{-1} due to C-O-C str. The ^{1}HNMR spectra of compounds 3a-3g showed peaks at δ10.13-10.16, 7.29-7.38, 6.25, 5.02 and 2.26 attributable to N-H, NH_2, furylring, CH-pyridine ring and CH_3 protons, respectively. The ^{13}CNMR spectra of compounds 3a-3g exhibited peaks at δ 169.6, 164.0 and 152.8-106.7 corresponding to the C-NH_2, oxadiazole and furyl ring. The FT-IR spectrum of the compounds (4a-4g) showed bands at 3345 to 3355 cm^{-1} due to N-H (pyridine ring) str, NH (triazole ring) absorption band at 3240 to 3252 cm^{-1}. The OH group in triazole ring absorbed at 3092-3082 cm^{-1}. The ^{1}HNMR spectrum of compounds 4a-4g showed peaks at δ 10.82, 5.82, 4.43, 2.50 attributable to OH, CH in pyridine ring, N-H(triazole), 2CH_3 in pyridine ring, respectively. The ^{13}CNMR spectrum of

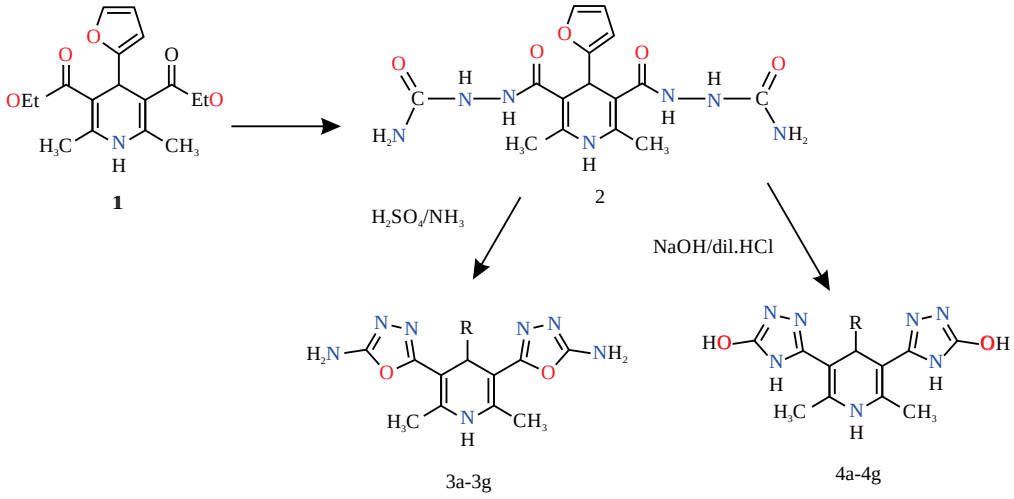

R = -furyl, -Ph, 4-ClC$_6$H$_4$, 4-OCH$_6$H$_4$, 4-NO$_2$C$_6$H$_4$, 4-CH$_3$OC$_6$H$_6$, 4-(CH$_3$), NC$_6$H$_4$

Scheme 1: Synthesis of 1,4-dihydropyridine derivatives (3a-3g and 4a-4g)

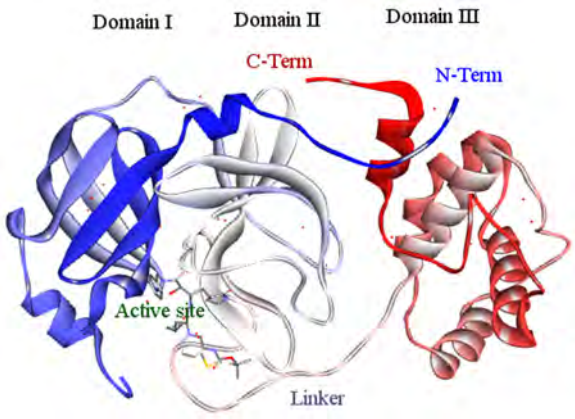

Fig. 1: Structural feature of the protease of SARS-CoV-2 M^{pro} composed of three domains

compounds 4a-4g exhibited peaks at δ 161.36, 146.40 and 15.92 corresponding to the C-OH, 2C in triazole ring and 2C in pyridine ring, respectively. The GC-MS (EI) spectra details given in experimental section.

Molecular simulation

Docking of target compounds and SARS-CoV-2 M^{pro} (PDB ID: 6y2f): The SARS-CoV-2 M^{pro} of corona virus is considered a major biological target for drugs and synthesized compounds. Figure 1 and Table 1 show the docking values of the pyridine analogues with protein as the lowest free energy ($\Delta G_{binding}$). Figure 1 shows structural protease of SARS-CoV-2 M^{pro} divides three domains and active site[35,36]. Table 2 represented the interaction between the compounds 3a-3g and SARS-CoV-2.

The docking energy ($G_{binding}$) was produced by AutoDock software (1.1.2 version, 1.5.6 application suite)+via sum of various factors as: $G_{binding} = G_{vdw}+G_{Gele}+G_h$ bond$+G_{desolv}+G_{tor}$ based on the lowest energy conformations. Based on substituents of the title compounds by furan(3a), benzene(3b), para-chlorobenzene(3c), phenol(3d), nitrobenzene(3e), anisole(3f) and N,N-dimethylaniline(3g) on pyridine ring. The binding energy of the docked compounds (3a-3g), remdesivir, hydroxychloroquine and chloroquine was observed at -5.89, -6.74, -6.58, -6.38, -6.76, -5.83, -5.54, -4.40, -5.22 and -5.41 Kcal mol^{-1}, respectively. So, all synthesized compounds significantly bind with SARS-CoV-2 M^{pro}, when match up to RDV, HQ and CQ. The contact between the 3a and SARS-CoV-2 M^{pro} was dominated by hydrogen bonds Thr A:199, Lys A:236 and Leu A:27 residues in site domain III. Molecular docking

Table 1: SARS-CoV-2 M^{pro} (PDB ID: 6y2f) docking results of the compounds 3a-3g and drugs (Unit: cal mol^{-1})

Compound	Estimated free energy of binding* (kcal mol^{-1})	Final intermolecular energy (kcal mol^{-1})	vdW+Hbond+desolv energy (kcal mol^{-1})	Electrostatic energy (kcal mol^{-1})	Final total internal energy (kcal mol^{-1})	Torsional free energy (kcal mol^{-1})	Unbound system's energy (kcal mol^{-1})
3a	-5.89	-7.38	-7.27	-0.10	-1.14	1.49	-1.14
3b	-6.74	-8.23	-7.80	-0.43	-0.68	1.49	-0.68
3c	-6.58	-8.07	-7.89	-0.18	-1.16	1.49	-1.16
3d	-6.38	-8.07	-7.89	-0.18	-1.16	1.49	-1.16
3e	-6.76	-8.55	-7.76	-0.79	-0.93	1.74	-0.93
3f	-5.83	-7.62	-7.48	-0.13	-1.34	1.79	-1.34
3g	-5.54	-7.33	-7.29	-0.04	-1.41	1.79	-1.41
RDV	-4.40	-9.47	-9.31	-0.16	-5.26	-5.07	-5.26
HQ	-5.22	-8.21	-7.28	-0.93	-0.71	2.98	-0.71
CQ	-5.41	-7.79	-7.30	-0.49	-0.66	2.39	-0.66

studies indicate the forming Van der Waals interaction between furan ring of compound 3a and domain III of receptor. The benzene of compound 3b formed two hydrogen bonds with Lys A:97 and Gln A:69 residues in domain I. The Pi-alkyl, alkyl and Pi cation interactions of Ala A:70 and Lys A:97 residues were suggested between aromatic ring of benzene and receptor for 3b. The data of 3c showed that 3c interacted with SARS-CoV-2 M^{pro} by hydrogen bonding of Gln A:19, Gly A: 71, Ser A:121, Lys A:97 and Gly A: 11 residues. The Pi-alkyl and alkyl interactions of Trp A:31 and Ala A:70 residues were suggested between aromatic ring of benzene and receptor for 3c. The compound 3d was able to combine with SARS-CoV-2 M^{pro} by hydrogen bonding of Ala A:285, Leu A:287, Try A:237 and Thr A:199 residues in the domain III. Also, the phenol of compound 3d interacted with Leu A:287 of SARS-CoV-2 M^{pro} by Pi-alkyl, alkyl and hydrogen interactions. Compound 3e was docked into domain I by hydrogen interactions of Gln A:19, Gln A:69, Lys A:97 and Glu A:14 residues. In addition, the Van der Waals interaction was suggested between Ser A:121 residue and 3e. Molecular docking studies indicated the forming hydrogen interaction of (3f) with Try A:239 and Leu A:287 residues of receptor in the domain III. The anisole of (3f) was situated in the domain III using Van der Waals interaction to Asn A:238 of receptor. The combine between the (3g) and SARS-CoV-2 M^{pro} was dominated by hydrogen bonds Leu A:287 and Tyr A:239 in the domain III. N, N-dimethylaniline of (3g) interacted into Asn A:238 of receptor using Van der Waals interaction.

The RDV may contribute hydrogen, Van der Waals, Pi-alkyl, alkyl and Pi-Pi T shaped combine in the domain III of SARS-CoV-2 M^{pro}. In addition, the HQ may contribute hydrogen, Pi-donor hydrogen, Van der Waals, Pi-alkyl, alkyl and Pi-sigma interactions in the domain III of SARS-CoV-2 M^{pro} and the CQ was formed via hydrogen, Pi-donor hydrogen and Van der Waals, Pi-alkyl and alkyl combine in the domain I of SARS-CoV-2 M^{pro}. The bonding interactions of compound 3c, RDV, HQ and CQ with SARS-CoV-2 main protease (6y2f) were illustrated in Fig. 2. Remaining compounds (3a, 3b, 3d, 3e, 3f and 3g) interactions provided in supplementary file.

The results confirmed that the presence electron with drawing groups on benzene such as nitro and chloro-substitutions or free benzene enhancement of the inhibitory behavior on SARS-CoV-2 M^{pro}, meanwhile, compounds containing contributing electron donating groups on benzene such as methoxy, hydroxyl or amine contribute to the decrease the inhibitory activities[37]. Figure 3 demonstrate the docked conformation of the compounds 4a, 4b, 4e, 4f, RDV, HQ and CQ with SARS-CoV-2 M^{pro} as the lowest value ($\Delta G_{binding}$). The remaining compounds (4c, 4d and 4g) are provided in supporting information. Table 3 shows the docking values of the compounds (4a-4g).

Based on substituent's of the title compounds by furan(4a), benzene(4b), *p*-chlorobenzene (4c), phenol(4d), nitrobenzene(4e), anisole (4f) and N,N-dimethylaniline(4g) on pyridine ring, binding energies of the docked compounds (4a-4g), RDV, HQ and CQ were observed at -7.14, -6.62, -6.89, -6.60, -7.71, -6.55 and -6.52 Kcal mol^{-1}, respectively. The results showed all synthesized compounds displayed more toward RDV, HQ and CQ. All compounds are interacted with SARS-CoV-2 M^{pro}, thereby inhibitory effects of ligand (4e) on SARS-CoV-2 M^{pro} were formed mediated hydrogen bond with Leu A:287, Tyr A:239, Ala A:285, Thr A:199, Asn A:238, Van der Waals bond with Thr A:198, Met A:276, Pi-Pi T shaped bond with Tyr A:239, Pi sigma with Leu A:287, Pi-alkyl with Leu A:286, Leu A:272 in domain III. Moreover, the interaction between ligand(2b) and receptor was dominated by hydrogen bond and carbon hydrogen bond (Tyr A:237, Ala A:285, Asn A:238, Thr A:199), Pi-Alkyl (Pro A:803) and Van der Waals bond (Tyr A:239, Thr A:198, Gly A:275, Leu A:271, Leu A:272, Gly A:275), Pi sigma bond (Leu A:287) and Pi-alkyl bond (Leu A:286, Met A:276) in domain III. The docked conformation ligand(3c) into SARS-CoV-2 M^{pro} revealed in hydrogen bond (Ala A:285, Leu A:287, Thr A:199, Asn A:238), Van der Waals bond (Thr A:198, Met A:276, Tyr A:239, Tyr A:237, Leu A:272),

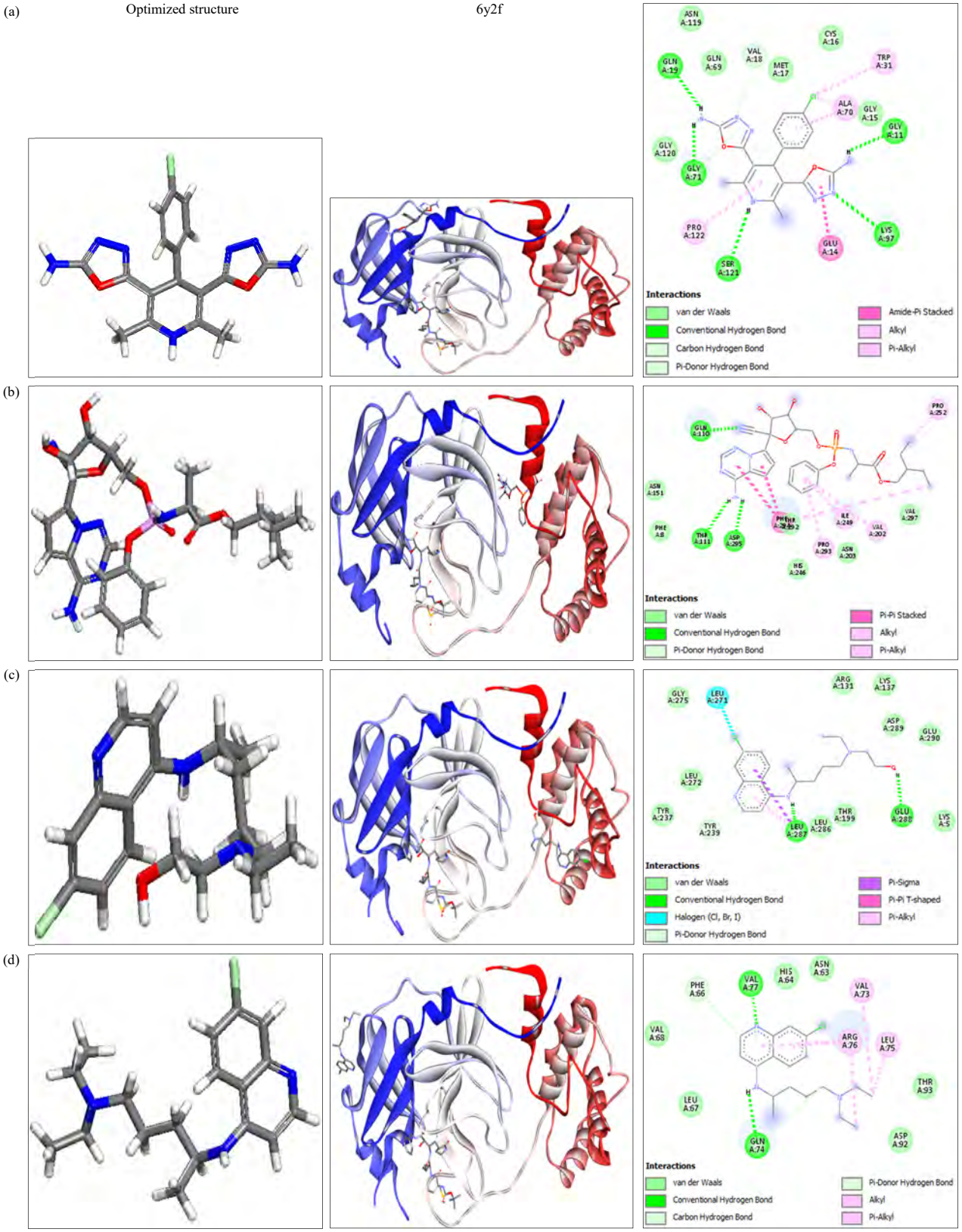

Fig. 2(a-d): Docking conformation of the synthesized compounds (a) 3c, (b) RDV, (c) HQ and (d) CQ with SARS-CoV-2 main protease (6y2f)

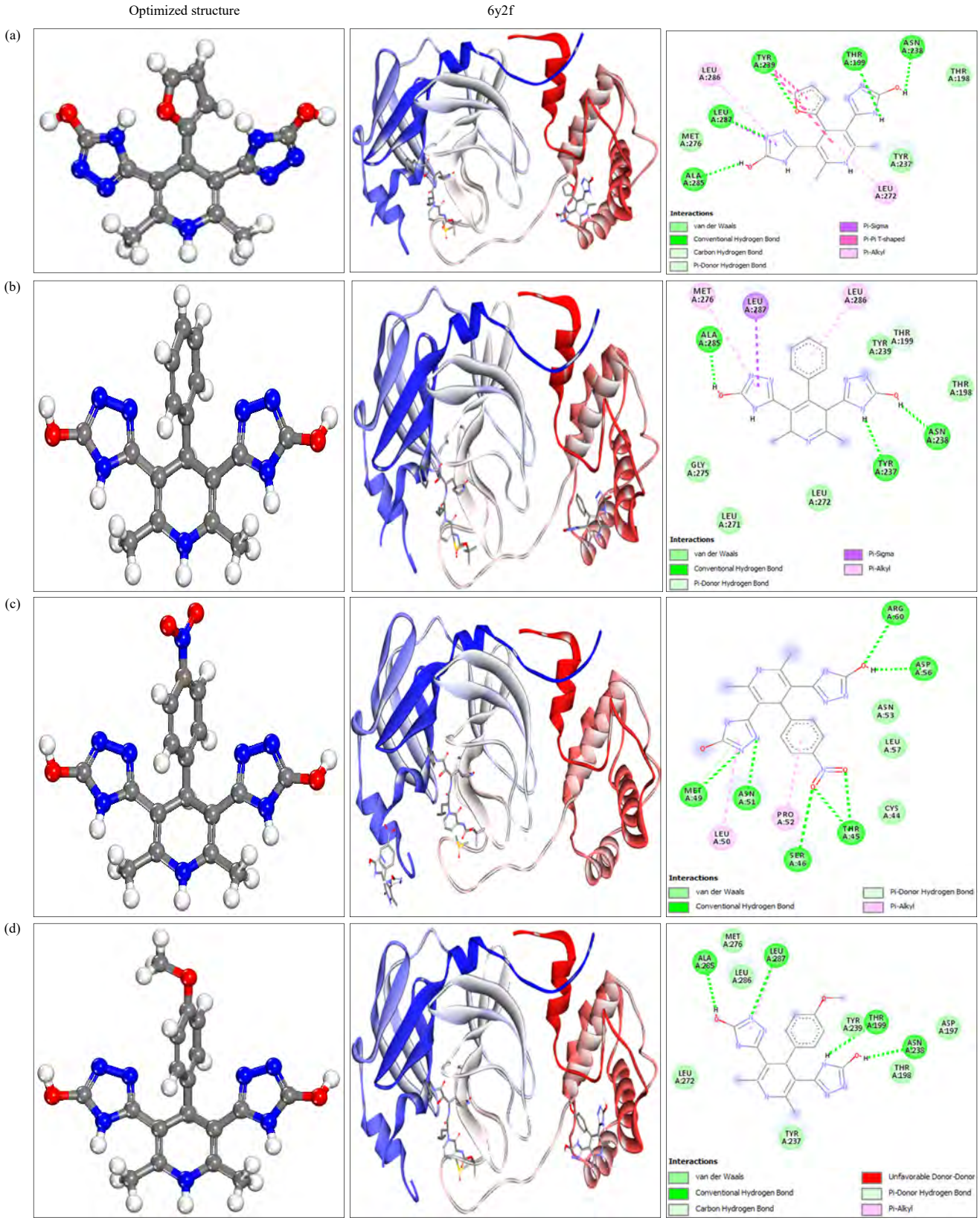

Fig. 3(a-d): Docking conformation of all synthesized compounds (a) 4a, (b) 4b, (c) 4e and (d) 4f with SARS-CoV-2 M^{pro} (6y2f)

Table 2: Interaction results between the compounds 3a-3g and drugs with SARS-CoV-2 M^{pro} (PDB ID: 6y2f)

Compound	Hydrogen, carbon hydrogen and Pi donor hydrogen bonds	Van der Waals interactions	Pi-Pi T shaped	Pi sigma	Pi-alkyl and alkyl	Amid Pi stack	P Sulfur
3a	Thr A:199, Lys A:236, Leu A:271	Asn A:238, Leu A:272, Gly A:275, Leu A:286	Tyr A:237	Leu A:287	Thr A:239		Met A:276
3b	Lys A:97, Gln A:69, Val A:18, Gly A:71	Trp A:31, Met A:17, Pro A:122, Asn A:119, Gln A:69, Ser A:121, Glu A:14, Pro A:121			Ala A:70	Gly A:120	
3c	Gln A:19, Gly A: 71, Ser A:121, Lys A:97, Gly A: 11, Val A:18, Cys A:16, Pro A:122,	Asn A:119, Gln A:69, Met A: 17,Gly A: 15, Gly A: 120			Trp A:31, Ala A:70	Gln A:14	
3d	Ala A:285, Leu A:287, Try A:237, Thr A:199	Leu A:287, Leu A:237, Leu A:199, Tyr A:239, Asn A:238, Leu A:272		Gly A:275	Leu A:287		Met A:276
3e	Gln A:19, Gln A:69, Lys A:97, Glu A:14, Gly A:71, Gly A:15, Pro A:122	Asn A:119, Ser A:121, Val A:18, Gly A:120, Asn A:95, Ala A:70, Met A:17, Trp A:31, Cys A:16					
3f	Try A:239, Leu A:287	Asp A:289, Val A:204, Thr A:199, Leu A:272, Ala A: 285, Met A:276, Leu A:271, Gly A: 275, Asn A:238	Tyr A:237	Leu A:286			
3g	Leu A:287, Tyr A:239	Val A:204, Thr A:199, Asp A:289, Asn A:238, Leu A:272, Ala A: 285, Met A: 276, Leu A:271, Gly A: 275	Tyr A:237	Tyr A: 237	Leu: A:286		
RDV	Gln A;110, Thr A;111, Asp A:295	Thr A:492, His A;246, Asn A:203, Val A:297, Phe A;8, Asn A:151	Phen A:282,	Ile A:249, Pro A:293, Val A;202, Pro A;252			
HQ	Glu A:288, Leu A:287, Tyr A:239	Asp A:289, Lys A:137, Arg A:131, Gly A:275, Leu A:272, Tyr A:237, Leu A:286, Thr A:199, Lys A:5, Glu A:290	Leu A:287	Leu A:287	Leu A:287		
CQ	Val A:77, Gln A:74, Phe A:66	Val A:68, His A:64, Asn A:63, Asp A:92, Thr A:93			Val A:73, Leu A:75, Arg A:76		

Table 3: SARS-CoV-2 M^{pro} (6y2f) docking results of the compounds 4a-4g (Unit: kcal mol^{-1})

Compound	Estimated free energy of binding* (kcal mol^{-1})	Final intermolecular energy (kcal mol^{-1})	vdW+Hbond+desolv energy (kcal mol^{-1})	Electrostatic energy (kcal mol^{-1})	Final total internal energy (kcal mol^{-1})	Torsional free energy (kcal mol^{-1})	Unbound system's energy (kcal mol^{-1})
4a	-7.14	-8.33	-8.12	-0.22	-0.47	1.19	-0.47
4b	-6.62	-8.12	-7.86	-0.26	-1.08	1.49	-1.08
4c	-6.89	-8.38	-8.17	-0.21	-1.17	1.49	-1.17
4d	-6.60	-8.39	-8.09	-0.30	-0.98	1.79	-0.98
4e	-7.71	-9.50	-8.28	-1.22	-1.21	1.79	-1.21
4f	-6.55	-8.34	-8.10	-0.23	-1.29	1.79	-1.29
4g	-6.52	-8.31	-8.11	-0.19	-1.03	1.79	-1.03

Pi sigma bond (Leu A:287) and Pi-alkyl bond (Leu A:286) in domain III. The docked conformation of ligand (3d) situated in SARS-CoV-2 M^{pro} via hydrogen bond (Leu A:287, Asn A:238, Thr A:237, leu A:271), Van der Waals bond (Leu A:286, Met A:276, Gly A:275, Thr A:193, Thr A:199, Glu A:288, Tyr A:237), Pi sigma bond (Leu A:287), as well as Pi-alkyl and alkyl bonds (Leu A:272, Tyr A:237).The docked conformation of ligand(3e) situated in SARS-CoV-2 M^{pro} via hydrogen bond (Met A:49, Asn A:51, Ser A:46, Thr A:45, Asp A:56, Arg A:60), Van der Waals bond (Asn A:53, Leu A:57, Cys A:44) and Pi-alkyl bond (Leu A:286) in domain I. In addition, ligand(3f) exhibited hydrogen interactions with Ala A:285, Leu A:287, Thr A:199, Asn A:238, Van der Waals bond (Asp A:197, Thr A:198, Met A:276, Tyr A:239, Tyr A:237, Leu A:272, Leu A:286) and Pi-alkyl bond (Leu A:287) in domain III. In addition, ligand(3g) exhibited hydrogen interactions with Ala A:285, Leu A:287, Thr A:199, Asn A:238, Van der Waals bond (Asp A:197, Thr A:198, Tyr A:237, Tyr A:239, Leu A:272, Leu A:286, Met A:276, Glu A:288) and Pi-alkyl bond (Leu A:287) in domain III.

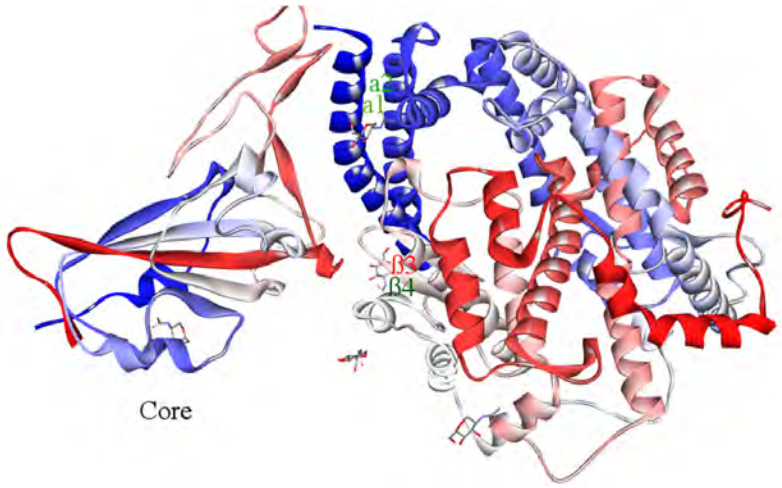

Fig. 4: Structural feature of the protease of ACE2

Table 4: ACE2 (6M0J) docking results of the compounds 3a-3g and drugs (Unit: kcal mol^{-1})

Compound	Estimated free energy of binding* (kcal mol^{-1})	Final Intermolecular energy (kcal mol^{-1})	vdW+Hbond+desolv energy (kcal mol^{-1})	Electrostatic energy (kcal mol^{-1})	Final total internal energy (kcal mol^{-1})	Torsional Free energy (kcal mol^{-1})	Unbound system's energy (kcal mol^{-1})
3a	-4.24	-5.74	-5.45	-0.29	-1.28	1.49	-1.28
3b	-4.67	-6.16	-5.88	-0.28	-1.41	1.49	-1.41
3c	-4.90	-6.39	-6.26	-0.13	-1.44	1.49	-1.44
3d	-4.16	-5.95	-5.54	-0.41	-1.21	1.79	-1.21
3e	-4.46	-6.24	-5.32	-0.92	-1.21	1.79	-1.21
3f	-2.54	-4.33	-4.25	-0.08	-1.45	1.79	-1.45
3g	-4.58	-6.37	-6.04	-0.33	-1.48	1.79	-1.48
RDV	-2.44	-7.51	-7.43	-0.08	-4.95	5.04	-4.95
HQ	-4.64	-7.62	-5.94	-1.68	-1.05	2.98	-1.05
CQ	-5.16	-7.55	-6.03	-1.52	-0.67	2.39	-0.67

Docking of compounds against ACE2 (6M0J): The coronaviruses attach to the spike (S) glycoprotein on the outer surface of the host cell's membrane. As a result, host cell target is for S1 subunit of the spike (S) glycol protein in corona viruses[38] 3D structure of ACE2 shows in Fig. 4. Figure 5 and Table 4 shows the molecular docking results and interactions of compounds 3c, RDV, HQ and CQ with ACE2 (6M0J). Remaining compounds 3a, 3b, 3d, 3e, 3f, 3g.

The minimum binding energies of compounds (3a-3g), RDV, HQ and CQ were -4.24, -4.67, -4.90, -4.16, -4.46, -2.54, -4.58, -2.44, -4.64 and -5.16 Kcal mol^{-1}, respectively. The CQ and ligand (3c) including Cl had more effect on ACE2 compared with other compounds and drugs.

The docking results of ligand (3c) with ACE2 showed ligands located inside pocket of hydrogen bond, Van der Waals, Pi-Pi T shaped and amid Pi stack relations. The ligand (3a) was participated in hydrogen interactions with Glu A:375, Pro A:346 in β3. Meanwhile, the ligand (3b) was participated in hydrogen interactions with Arg A:393, Tyr A:385, Ala A:348 and Glu A:375 in core section. The ligand(3c) was formed hydrogen bond, Van der Waals, Pi sigma, Pi-Pi T shaped, Pi-alkyl and unfavorable acceptor-acceptor interactions in β3 of ACE2. In addition, ligand(3d) can be accommodated by binding pocket of hydrogen bond, Van der Waals, Pi-cation and carbon hydrogen bond and form hydrogen bonds to Ser A:545, Asp A:543 and Asn A:546 of ACE2. Ligand(3e) was interacted with ACE2 via formation of hydrogen bond with Glu A:433, Gln A:287, Lys A:247 and Asp A:597 and Van der Waals interactions with Gly A:286, Phe A:285, Gln A:598, Trp A:594 and Pro A:284. Ligand(3f) bound to ACE2 with Ala A:522 and Leu 518 through hydrogen as well as Pro E521, Ala A:520, His E:519 and Leu E:390 bonding via Van der Waals interactions.

There are five kinds of hydrogen (Pro A:346, Glu A:375, Ala A:348), Van der Waals 9 His A:345, His A:378, His A:401, Tyr A:385, Asp A:382, Phe A:40, Ser A:43, Ser A:44, Asn A:51), carbon hydrogen (Thr A:347), Pi-Pi T shaped (Trp A:345), Pi-alkyl (Ala A:348) and amid-Pi stack (Asp A:350) interactions in the binding model of ligand(3g).

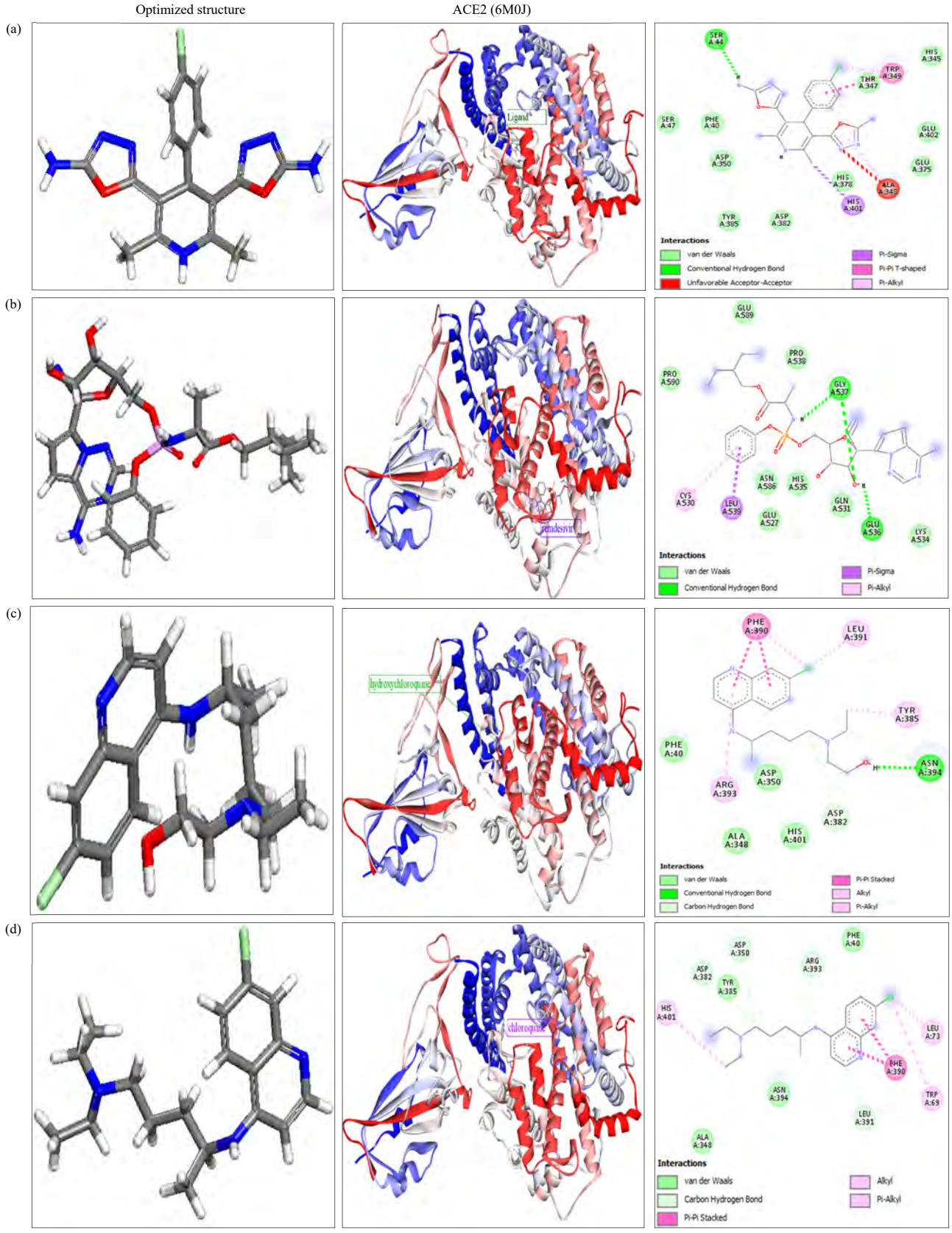

Fig. 5(a-d): Docking conformation of all synthesized compounds (a) 3c, (b) RDV, (c) HQ and (d) CQ with ACE2 (6M0J)

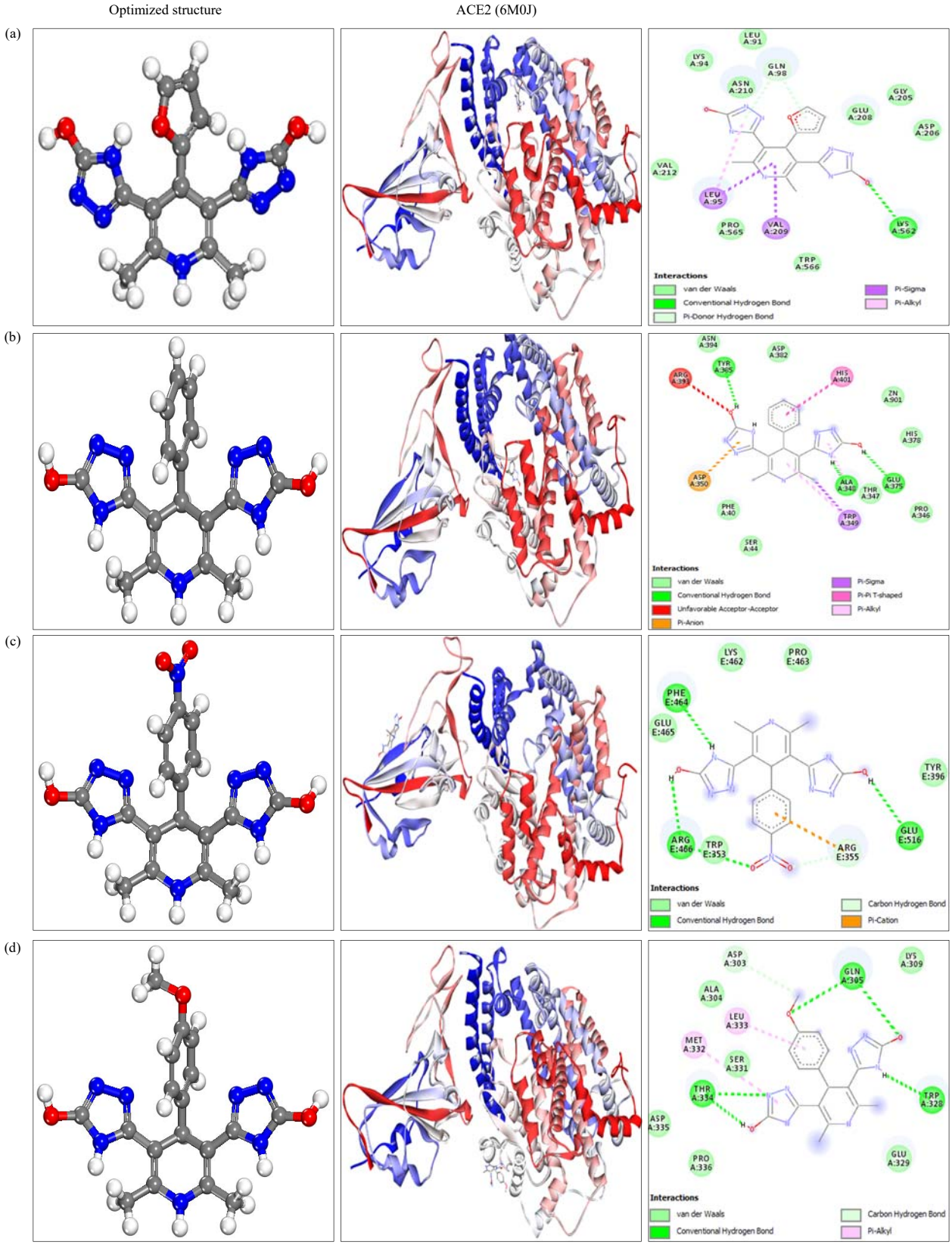

Fig. 6(a-d): Docking conformation of synthesized compounds (a) 4a, (b) 4b, (c) 4e and (d) 4f with ACE2 (6M0J)

The RDV interacted with ACE2 via formation of hydrogen bonds with Gly A:537 and Glu A:536, Van der Waals interactions with Glu A:539, Pro A:538, Pro A:590, Asn A:586, Glu A:527, His A:535, Gln A:531, Lys A:534, Pi sigma relations with Leu A:539 and Pi-alkyl interaction with Cys A:530.

The HQ interacted via the formation of hydrogen bonds of Asn A:394, Asp A:382, Van der Waals interactions with Phe A:40, Asp A:350, Ala A:348, His A:401, Asp A:382, Pi-alkyl and alkyl and Pi-Pi stack interactions in β3. In addition, chloroquine also interacted via the formation of H_2 bond, Van der Waals interactions, Pi-alkyl and alkyl and Pi-Pi stack interactions. The CQ was exhibited via the formation of hydrogen bond, Van der Waals interactions, Pi-alkyl and alkyl and Pi-Pi stack interactions (Fig. 6).

Based on substituents of the title compounds by furan(4a), benzene(4b), para chlorobenzene(4c), phenol(4d), nitrobenzene(4e), anisole(4f) and N,N-dimethylaniline(4g) on pyridine ring, binding energies of the docked ligands (4a), (4b), (4c), (4d), (4e), (4f), (4g), remdesivir, hydroxychloroquine and chloroquine with ACE2 were observed as -5.90, -4.72, -4.62, -4.42, -4.87, -4.90 and -4.87 Kcal/mol, respectively. Chloroquine and ligand(4a) had more effect on ACE2 compared with other compounds and drugs.

Ligand(4a) interacted with ACE2 via formation of hydrogen and Pi-donor hydrogen bond with Lys A:562, Gln A:98, Van der Waals interactions with Lys A:94, Leu A:91, Asn A:210, Glu A:208, Gly A:205, Asp A:206, Tyr A:385, Trp A:556, Pro A:565, Val A:212, Pi-sigma Leu A:95, Val A:209 and Pi-alkyl interaction with Leu A:95. Ligand(4b) was docked into β3 of ACE2 by hydrogen interactions of Tyr A:385, Ala A:348, Glu A:375 residues. Ligand(4c) was also surrounded by Van der Waals, hydrogen, Pi-Pi T shaped, Pi sigma and alkyl interactions in β3 section.

Ligand (4d) was involved in hydrogen, Van der Waals, Pi-Pi stacked and Pi-alkyl connections with receptor ACE2 in the α2 section. In addition, ligand(4e) was involved in the binding of hydrogen, carbon hydrogen bond, Pi-cation interactions in the core section. Ligand (4f) also is presented in pocket of hydrogen, carbon hydrogen bonds and Pi-alkyl interactions with receptor ACE2 in the β4 section. Three types of hydrogen bonds, Van der Waals, Pi-Pi T shaped, Pi-alkyl and Pi sigma interactions were observed between ligand(4f) and ACE2 in β4 section. Ligand(4g) was exhibited to interact via formation of hydrogen bond with Ser A:44, Ala A:348, hydrophobic interactions with Tyr A:385, Phe A:350, Asp A:350, Asp A:382, His A:378, Thr A: 347, Glu A: 375, Glu A: 402, Van der wall interactions with Tyr A:385, Phe A:350, Asp A:350, Asp A:382, His A:378, Thr A: 347, Glu A: 375, Glu A: 402, Pi-Pi T shaped interaction with Trp A:349, Pi-alkyl interaction with Ala A:348 and Pi sigma interaction with His A:401.

CONCLUSION

A novel approach for the high yield of new 1,4-dihydropyridine derivatives (3a-3g and 4a-4g) were studied and Dmol3Module's 2017 Materials Studio software was used to optimize the shape of the compounds. The *in silico* study of optimized structures was used for the protease of SARS-CoV-2 M^{pro} (PDB ID: 6y2f) and ACE2 (6M0J). Due to the interaction of all synthesized compounds on domain I and II in protease of SARS-CoV-2 M^{pro}, the lowest energy conformations were created, hence 3a-3g and 4a-4g can be used as antagonists compared to other drugs to kill corona virus. The compound (4a) has interacted with the α2 ACE2 receptor. The synthesized compounds (3c), (4a), (4b), (4e) and (4f) were found to have potential anticoronavirus activity in the section of SARS-CoV-2 M^{pro}. To determine if the compounds are useful as clinical antiviral agents, *in vitro* studies will be conducted.

SIGNIFICANCE STATEMENT

The purpose of this work was to discover new 1,4-dihydropyridine derivatives and used for antiviral drug, lesser reaction time. The key finding of the study shows that the compounds 3c, 4a, 4b, 4e and 4f exhibited good interaction with ACE2 receptor and used for further antiviral activity study. The findings suggested that the newly synthesized compounds are further evaluation for SARS-CoV-2 drug.

ACKNOWLEDGMENTS

The authors are thankful to the Department of Science and Technology, Government of India for providing DST-FIST fund (SR/FST/COLLEGE-372/2018) to Nehru Memorial College, Puthanampatti, Trichy, Tamil Nadu, India under the FIST program. The authors extend their appreciation to the Researchers supporting project number (RSPD2023R543) King Saud University, Riyadh, Saudi Arabia.

REFERENCES

1. Haribabu, J., S. Srividya, D. Mahendiran, D. Gayathri, V. Venkatramu, N. Bhuvanesh and R. Karvembu, 2020. Synthesis of palladium(II) complexes via michael addition: Antiproliferative effects through ROS-mediated mitochondrial apoptosis and docking with SARS-CoV-2. Inorg. Chem., 59: 17109-17122.

2. Zhu, N., D. Zhang, W. Wang, X. Li and B. Yang *et al*., 2020. A novel coronavirus from patients with pneumonia in China, 2019. N. Engl. J. Med., 382: 727-733.
3. Mitsuya, H. and N. Kokudo, 2020. Sustaining containment of COVID-19: Global sharing for pandemic response. Global Health Med., 2: 53-55.
4. Livingston, E. and K. Bucher, 2020. Coronavirus disease 2019 (COVID-19) in Italy. JAMA, Vol. 323. 10.1001/jama.2020.4344.
5. Li, Q., X. Guan, P. Wu, X. Wang and L. Zhou *et al*., 2020. Early transmission dynamics in Wuhan, China, of novel coronavirus-infected pneumonia. N. Engl. J. Med., 382: 1199-1207.
6. Liu, C., Q. Zhou, Y. Li, L.V. Garner and S.P. Watkins *et al*., 2020. Research and development on therapeutic agents and vaccines for COVID-19 and related human coronavirus diseases. ACS Cent. Sci., 6: 315-331.
7. Burki, T.K., 2020. The Russian vaccine for COVID-19. Lancet Respir. Med., 8: E85-E86.
8. Xu, J., S. Zhao, T. Teng, A.E. Abdalla and W. Zhu *et al*., 2020. Systematic comparison of two animal-to-human transmitted human coronaviruses: SARS-CoV-2 and SARS-CoV. Viruses, Vol. 12. 10.3390/v12020244.
9. Hilgenfeld, R., 2014. From SARS to MERS: Crystallographic studies on coronaviral proteases enable antiviral drug design. FEBS J., 281: 4085-4096.
10. Gorbalenya, A.E. and E.J. Snijder, 1996. Viral cysteine proteinases. Perspect. Drug Discovery Des., 6: 64-86.
11. Muramatsu, T., C. Takemoto, Y.T. Kim, H. Wang and W. Nishii *et al*., 2016. SARS-CoV 3CL protease cleaves its C-terminal autoprocessing site by novel subsite cooperativity. Proc. Natl. Acad. Sci. U.S.A., 113: 12997-13002.
12. Dai, W., B. Zhang, X.M. Jiang, H. Su and J. Li *et al*., 2020. Structure-based design of antiviral drug candidates targeting the SARS-CoV-2 main protease. Science, 368: 1331-1335.
13. Marinescu, M. and C.V. Popa, 2022. Pyridine compounds with antimicrobial and antiviral activities. Int. J. Mol. Sci., Vol. 23. 10.3390/ijms23105659.
14. Malhotra, M., S. Sharma and A. Deep, 2012. Synthesis, characterization and antimicrobial evaluation of novel derivatives of isoniazid. Med. Chem. Res., 21: 1237-1244.
15. Triggle, D.J., 2003. 1,4-Dihydropyridines as calcium channel ligands and privileged structures. Cell. Mol. Neurobiol., 23: 293-303.
16. Alker, D., S.F. Campbell, P.E. Cross, R.A. Burges, A.J. Carter and D.G. Gardiner, 1990. Long-acting dihydropyridine calcium antagonists. 4. Synthesis and structure-activity relationships for a series of basic and nonbasic derivatives of 2[(2-aminoethoxy)methyl]-1,4-dihydropyridine calcium antagonists. J. Med. Chem., 33: 585-591.
17. Vijesh, A.M., A.M. Isloor, S.K. Peethambar, K.N. Shivananda, T. Arulmoli and N.A. Isloor, 2011. Hantzsch reaction: Synthesis and characterization of some new 1,4-dihydropyridine derivatives as potent antimicrobial and antioxidant agents. Eur. J. Med. Chem., 46: 5591-5597.
18. Shahrisa, A., R. Miri, S. Esmati, M. Saraei, A.R. Mehdipour and M. Sharifi, 2012. Synthesis and calcium channel antagonist activity of novel 1,4-dihydropyridine derivatives possessing 4-pyrone moieties. Med. Chem. Res., 21: 284-292.
19. Kappe, C.O., W.M.F. Fabian and M.A. Semones, 1997. Conformational analysis of 4-aryl-dihydropyrimidine calcium channel modulators. A comparison of ab initio, semiempirical and X-ray crystallographic studies. Tetrahedron, 53: 2803-2816.
20. Yamamoto, T., S. Niwa, S. Ohno, M. Tokumasu and Y. Masuzawa *et al*., 2008. The structure-activity relationship study on 2-, 5-, and 6-position of the water soluble 1,4-dihydropyridine derivatives blocking N-type calcium channels. Bioorg. Med. Chem. Lett., 18: 4813-4816.
21. Mauzerall, D. and F.H. Westheimer, 1955. 1-Benzyldihydronicotinamide-A model for reduced DPN. J. Am. Chem. Soc., 77: 2261-2264.
22. Boecker, R.H. and F.P. Guengerich, 1986. Oxidation of 4-aryl- and 4-alkyl-substituted 2,6-dimethyl-3,5-bis(alkoxycarbonyl)-1,4-dihydropyridines by human liver microsomes and immunochemical evidence for the involvement of a form of cytochrome P-450. J. Med. Chem., 29: 1596-1603.
23. Kumar, R.S., A. Idhayadhulla, A.J. Abdul Nasser and J. Selvin, 2011. Synthesis and anticoagulant activity of a new series of 1,4-dihydropyridine derivatives. Eur. J. Med. Chem., 46: 804-810.
24. Miri, R. and A. Mehdipour, 2008. Dihydropyridines and atypical MDR: A novel perspective of designing general reversal agents for both typical and atypical MDR. Bioorg. Med. Chem., 16: 8329-8334.
25. Wan, J.P. and Y. Liu, 2012. Recent advances in new multicomponent synthesis of structurally diversified 1,4-dihydropyridines. RSC Adv., 2: 9763-9777.
26. Forrestall, K.L., D.E. Burley, M.K. Cash, I.R. Pottie and S. Darvesh, 2021. 2-Pyridone natural products as inhibitors of SARS-CoV-2 main protease. Chem. Biol. Interact., Vol. 335. 10.1016/j.cbi.2020.109348.
27. Bosica, G. and R. Abdilla, 2022. Recent advances in multicomponent reactions catalysed under operationally heterogeneous conditions. Catalysts, Vol. 12. 10.3390/catal12070725.
28. Viradiya, D., S. Mirza, F. Shaikh, R. Kakadiya and A. Rathod *et al*., 2017. Design and synthesis of 1,4-dihydropyridine derivatives as anti-cancer agent. Anti-Cancer Agents Med. Chem., 17: 1003-1013.

29. Olejníková, P., Ľ. Švorc, D. Olšovská, A. Panáková, Z. Vihonská, K. Kovaryová and A. Marchalín, 2014. Antimicrobial activity of novel C2-substituted 1,4-dihydropyridine analogues. Sci. Pharm., 82: 221-232.
30. Razzaghi-Asl, N., R. Miri and O. Firuzi, 2016. Assessment of the cytotoxic effect of a series of 1,4-dihydropyridine derivatives against human cancer cells. Iran. J. Pharm. Res., 15: 413-420.
31. Elsayed, S.A., A.M. El-Hendawy, S.I. Mostafa, B.J. Jean-Claude, M. Todorova and I.S. Butler, 2010. Antineoplastic activity of new transition metal complexes of 6-methylpyridine-2-carbaldehyde-N(4)-ethylthiosemicarbazone: X-ray crystal structures of [Vo2(mpETSC)] and [PT(mpETSC)CL]. Bioinorg. Chem. Appl., Vol. 2010. 10.1155/2010/149149.
32. Byrkit, G.D. and G.A. Michalek, 1950. Hydrazine in organic chemistry. Ind. Eng. Chem., 42: 1862-1875.
33. Agarwal, R.K., S. Prasad and N. Gahlot, 2004. Synthesis, spectral and thermal properties of some penta-coordinated complexes of oxovanadium(IV) derived from thiosemicarbazones of 4-aminoantipyrine. Turk. J. Chem., 28: 691-702.
34. Kumar, S.R., A. Idhayadhulla, A.J.A. Nasser and J. Selvin, 2011. Synthesis and antimicrobial activity of a new series 1,4-dihydropyridine derivatives. J. Serbian Chem. Soc., 76: 1-11.
35. Kumar, Y., H. Singh and C.N. Patel, 2020. *In silico* prediction of potential inhibitors for the main protease of SARS-CoV-2 using molecular docking and dynamics simulation based drug-repurposing. J. Infect. Public Health, 13: 1210-1223.
36. El-Sherief, H.A.M., B.G.M. Youssif, S.N.A. Bukhari, A.H. Abdelazeem, M. Abdel-Aziz and H.M. Abdel-Rahman, 2018. Synthesis, anticancer activity and molecular modeling studies of 1,2,4-triazole derivatives as EGFR inhibitors. Eur. J. Med. Chem., 156: 774-789.
37. Basu, A., A. Sarkar and U. Maulik, 2020. Molecular docking study of potential phytochemicals and their effects on the complex of SARS-CoV2 spike protein and human ACE2. Sci. Rep., Vol. 10. 10.1038/s41598-020-74715-4.
38. Rathod, S.B., P.B. Prajapati, L.B. Punjabi, K.N. Prajapati, N. Chauhan and M.F. Mansuri, 2020. Peptide modelling and screening against human ACE2 and spike glycoprotein RBD of SARS-CoV-2. *In silico* Pharmacol., Vol. 8. 10.1007/s40203-020-00055-w.